

PCCP

Accepted Manuscript



This is an *Accepted Manuscript*, which has been through the Royal Society of Chemistry peer review process and has been accepted for publication.

Accepted Manuscripts are published online shortly after acceptance, before technical editing, formatting and proof reading. Using this free service, authors can make their results available to the community, in citable form, before we publish the edited article. We will replace this *Accepted Manuscript* with the edited and formatted *Advance Article* as soon as it is available.

You can find more information about *Accepted Manuscripts* in the [Information for Authors](#).

Please note that technical editing may introduce minor changes to the text and/or graphics, which may alter content. The journal's standard [Terms & Conditions](#) and the [Ethical guidelines](#) still apply. In no event shall the Royal Society of Chemistry be held responsible for any errors or omissions in this *Accepted Manuscript* or any consequences arising from the use of any information it contains.

Protic Ionic Liquids (PILs) Nanostructure and Physicochemical Properties: Development of High-Throughput Methodology for PIL Creation and Property Screens

Tamar L. Greaves,^{a,b*} Krystal Ha^{a,b}, Benjamin W. Muir^c, Shaun C Howard^c, Asoka Weerawardena^{a,b}, Nigel Kirby,^d Calum J. Drummond^{a,b}

^a School of Applied Sciences, College of Science, Engineering and Health, RMIT University, GPO Box 2476, Melbourne, Victoria 3001, Australia.

^b CSIRO Manufacturing Flagship, Bag 10, Clayton, Vic. 3169, Australia.

^c CSIRO Rapid Automated Materials & Processing Centre, Manufacturing Flagship, Bag 10, Clayton, Vic. 3169, Australia.

^d Australian Synchrotron, 800 Blackburn Road, Clayton, Victoria 3168 (Australia)

* Corresponding author. Email: tamar.greaves@rmit.edu.au

Abstract

A high-throughput approach was developed in order to prepare and dry a series of protic ionic liquids (PILs) from 48 Brønsted acid-base combinations. Many combinations comprised an alkyl carboxylic acid paired with an alkyl amine. Visual screens were developed to identify which acid-base combinations formed PILs, and of those, which PILs were likely to have high surface tensions, low viscosities, and low melting points. The surface tension screen was validated through pendant drop surface tension measurements. Karl Fischer coulometric titration was used to obtain the water contents, and it was noted that there is a considerable difference in the drying rate throughout this series of PILs. It was observed that an octyl chain present on either the cation or anion was detrimental to the formation of a PIL with a low melting point, and instead increased the likelihood of a gel or solid forming. The nanostructure of the PILs was determined, using synchrotron small and wide angle X-ray scattering (SAXS/WAXS), to consist of polar and non-polar domains, with the alkyl chains on the cation and anion intercalating. The results indicate that both the alkyl chain on the cation and/or anion contribute to the correlation distance, for the intermediate range order, with the expectation that there is charge alternation of the ions in the polar region. The maximum correlation distance was observed when there was an alkyl chain present on only one ion. This correlation distance could be significantly reduced by varying the alkyl chain length present on the other ion, which was attributed to increased disorder and interdigitation of chains, and to toe-to-toe alignment of the chains. To the best of our knowledge this is the first PIL report into the effect of having an alkyl chain present on both the cation and the anion.

Introduction

Ionic liquids (ILs) are recognised as tailorable solvents due to the vast number of potential cation and anion combinations. The solvent properties most commonly of interest are melting point, thermal stability, viscosity, conductivity, electrochemical window, surface tension, toxicity, environmental impact and cost.¹⁻³

The selection and optimisation of ILs for specific applications can be difficult due to the need to trial a wide variety of existing ILs and potentially to synthesise new ILs. In addition, for many applications the addition of molecular solvents or other ILs can be beneficial to the overall solvent properties.⁴ Consequently, the selection of an IL for a specific application is often multi-dimensional encompassing the choice of cation, anion and additional solvents.

High-throughput (HT) techniques are routinely used in the drug discovery process by utilising automation to efficiently assay a large number of drugs, thereby significantly decreasing the cost and time required to develop new therapeutic candidates.⁵ There is a need for HT approaches to IL synthesis and in the screening of ILs and IL-solvents to allow the rapid identification of potential ILs for specific applications. To date, the development and trialling of ILs for specific applications reported in the literature typically involves a small number of ILs, with little ion variation, though there have been some larger sets such as the work of Watanabe et al. where nearly 40 PILs were investigated for use as electrolytes in fuel cells.⁶ To the best of our knowledge, the only HT screens which have been reported for ILs screen for biocompatibility using an Agar Diffusion test⁷, and for the ability of the ILs to dissolve lingo-cellulose using extinction or light scattering measurements⁸.

Protic Ionic Liquids (PILs) are a subset of ILs which are produced through proton transfer from a Brønsted acid to a Brønsted base.³ The synthesis of PILs requires a simple equimolar acid-base reaction, followed by drying,⁹ making them generally the simplest and cheapest ILs to synthesise. The synthesis method is similar for many PILs, and hence they are particularly well suited for HT preparation.

While aprotic ILs have a significantly more complicated synthesis, it is still viable to prepare a series of ILs in a HT manner where the synthesis steps are consistent. The use of high-throughput screens is valid for the rapid identification of ILs and IL-solvent mixtures for both PILs and aprotic ILs. This approach has the potential to take this field from investigating typically less than 50 ILs or IL-solvent mixtures, and increasing it to thousands within similar timeframes.

In this HT investigation we have utilised a Chemspeed robotic platform equipped with ISYNTH reactor blocks to synthesise and dry a series of 48 acid-base combinations. To the best of our knowledge this is the first report of a scalable high-throughput preparation methodology for ILs. In addition, simple HT screens have been utilised to enable identification of beneficial solvent properties, including likelihood of low melting points, surface tension and viscosity. The surface tension screen was validated using conventional surface tension measurements. The acid-base combinations were selected to produce 48 combinations, of which 13 have previously been reported in the literature. The overlap with existing PILs was deliberate to enable comparison of the properties between those synthesised in a high-throughput and a conventional manner. The liquid nanostructure of the PILs were characterised using synchrotron SAXS/WAXS.

Experimental Method

The chemicals were all used as received. Ethanolamine (Sigma-Aldrich, 99.5%), ethylamine (Aldrich, 70 wt% in solution of water), propylamine (Merck, 100%), pentylamine (Merck, 98%), hexylamine (Merck, 100%), octylamine (Aldrich, 99%), nitric acid (Merck, 70%), formic acid (Merck, 98%), acetic

acid (Merck, 100%), propionic acid (ChemSupply, 99.5%), pentanoic acid (99%, Sigma-Aldrich), hexanoic acid (Aldrich, 99%), heptanoic acid (Sigma-Aldrich, 99%), octanoic acid (Sigma-Aldrich, 99%), Methanol (Merck). Butylamine and butanoic acid were omitted from the series due to their strong chemical odor.

Karl Fischer Titration. The water content of the dried PILs was determined using Karl Fischer coulometric titration. Typically 0.4 mL of 10 w/w % solution of the salt in diluted anhydrous methanol was injected for analysis.

Surface tensions were measured using a SITA t60 Bubble tensiometer.

Small- and wide-angle X-ray scattering experiments (SAXS/WAXS) were performed on the SAXS/WAXS beamline at the Australian Synchrotron, Clayton, Australia. Liquid samples were loaded into 1.5 mm capillaries and sealed with a silicon rubber to prevent water absorption, and solid samples were loaded into a 96 well plate. The temperature of the sample holder was controlled using a Huber recirculating water bath. Scattering patterns were acquired at temperatures of 25 and 60 °C using an exposure time of 1 s, and a wavelength of $0.827 \times 10^3 \text{ \AA}$. The SAXS q range was $0.03\text{--}0.63 \text{ \AA}^{-1}$, and the WAXS q range was from 0.6 to 2.58 \AA^{-1} . The contribution from an empty capillary or empty well in the plate was subtracted from the scattering profiles. The capillaries were nominally 1.5 mm diameter; however, there were some small deviations in size which may lead to changes in the intensities of a few percent. The SAXS and WAXS data were carefully combined to obtain profiles with the q range of $0.03\text{--}2.58 \text{ \AA}^{-1}$.

Chemspeed Robotic Platform Synthesis.

The IL synthesis was conducted using a Chemspeed robotic synthesis platform which contained an ISYNTH reactor block equipped with an array of 24 vials holding a maximum volume of 20 mL each. The protocol was designed to mimic the conventional synthesis of protic ionic liquids, with methanol added to the base (stock) solutions, to ensure a liquid state during addition of the acid. The quantities of the methanol-amine stock solutions are provided in Table S1 of the supplementary information.

The robotic platform dispenses (low-viscosity) liquids by means of an articulated 4-needle tool connected to four individual syringe pumps which allow concurrent aspiration/dispensing of amines or acids to/from four adjacent vials. Each syringe pump can operate individually to deliver different volumes, and at different rates to the other syringes. In this particular application, the platform was fitted with four 10mL syringe pumps, and four stainless steel needles (ID=0.8 mm). The synthesis was conducted in two sequential batches of 24 IL mixtures. The basic experimental steps programmed into the Chemspeed workflow for each batch are described below. The programmed volumes for each base and acid can be found in Table S2 of the supplementary information.

1. Reagent bases (amine+methanol) and acids were loaded into 60mL reservoir vials and fitted with purge septa.
2. ISYNTH reactors were configured to be open under inert atmosphere (to prevent condensation) and cooled to a target temperature of 0°C.

- Each of the six amine-methanol mixtures were sequentially dispensed to four ISYNTH reactor vials such that all 24 reactor vials contained amine. Amines were aspirated at 5 mL/min and dispensed at 20 mL/min.
- Agitation/shaking of reactors was turned on (400 RPM).
- Each of the four acids were then added drop-wise to four ISYNTH reactors such that all 24 reactor vials contained acid+base. Acids were aspirated at 10 mL/min and dispensed at 0.1 mL/min to achieve dropwise addition over an extended period of time.
- The reactors were agitated for an additional hour following the final acid addition. Due to the dropwise addition of acid, all reactions had sufficient time to react of between 2 and 6 hours.
- ISYNTH reactors were configured to be closed. Vacuum pressure in the reactors was stepped down gradually to a target pressure of 1 mbar on the attached vacuum pump. At the same time the temperature was set to 38°C (43°C on attached cryostat).
- Vacuum, heat, and agitation were continued for approximately 48 hours, although review of log data indicates that minimal pressure was obtained within 2 hours of starting step 7.
- Pressure and temperature were returned to ambient conditions before the 24 reactor vials were removed, capped and taken away for analysis.
- Steps 1-9 were repeated for batch 2, which used the same six bases, and the four remaining acids.

The 48 Brønsted acid-base combinations were simultaneously further dried at 70-80 °C in a vacuum oven for approximately 25 hours.

Results

The series of 48 acid-base combinations were prepared and dried using the ChemSpeed robotic platform. The visual appearance of the samples is provided in the supplementary material in Figure S1. A simple visual screen was used to classify the state of the samples as liquid, solid or gel, which can be clearly observed for the octylamine + acid series shown in Figure 1. The final volumes of the samples should be comparable based on the initial volumes used, so an acid-base combination where there is a significantly smaller volume indicates volatility (after drying), and hence poor proton transfer from the acid to the base. Of the 48 acid-base combinations only 3 had a low volume after drying, which were pentylamine + octanoic acid, ethanolamine + octanoic acid and octylamine + nitric acid. Of these, the first two combinations had low volume after the drying on the chemspeed at 38 °C, whereas the octylamine + nitric acid only had low volume after the final drying in the vacuum oven. It is reasonable to assume that the remaining 45 combinations had at least reasonable proton transfer to achieve a low volatility.

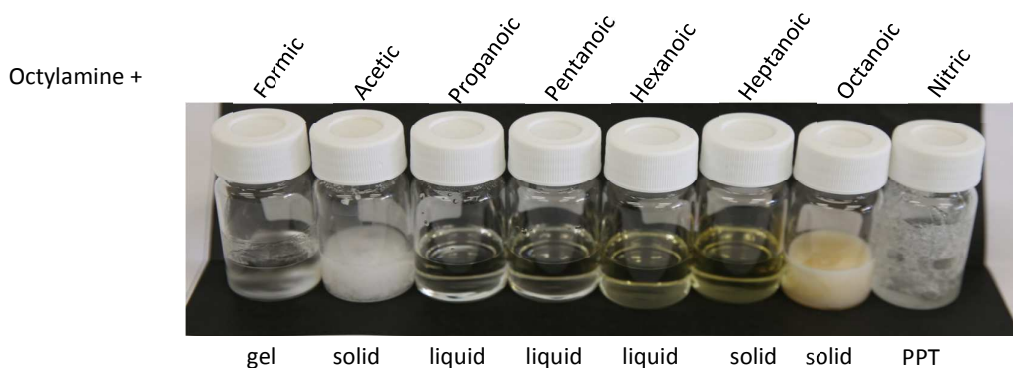


Figure 1. Acid-base combinations for octylamine with each of the acids. These are classified based on visual inspection as liquid, solid, gel or poor proton transfer (PPT).

A summary of the visual state of the samples is provided in Figure 2 as a heat map, along with the names and structures of the acid and base precursors. For the liquid samples, an indication of the viscosity was obtained through a simple screen by turning the vials upside down and observing how long the liquid took to fall. The viscosity was classified as low (L), medium (M) or high (H), provided in Figure 2, with high viscosities corresponding to little movement of sample within 20 seconds when upside down, medium viscosities to less than 20 seconds for liquid to return to bottom of vial, and low viscosities comparable to water.

The viscosity increased as the alkyl chain length on either the anion or the cation increased, or through the addition of the hydroxyl on the ethanolamine compared to ethylamine. This is consistent with what has previously been observed for alkylammonium carboxylate PILs, where the increasing alkyl chain lengths increase van der Waals interactions between the alkyl chains, and hydroxyl groups increase the amount of hydrogen bonding present.⁹ It has previously been observed for PILs^{3,9} and aprotic ILs¹⁰ that changes to the anion structure has a greater influence on the viscosity than similar changes to the cation. While the viscosity screen used here does not include absolute values, the relative changes observed are consistent with the literature.

It is apparent that having an octyl chain on either the amine or the acid is highly detrimental to the likelihood of forming PILs with desirable low melting points. From Figure 2 it can be observed that of the 8 acid-base combinations including octylamine, only three were liquid at room temperature, and similarly of the 6 acid-base combinations which included octanoic acid, only two were liquid at room temperature. We note that the hexyl and heptyl alkyl chains on the amine or acid did not appear to affect the overall sample in the same way as the octyl chains. The prevalence of gel and solid samples containing the octyl chain, but not the heptyl or hexyl, suggests that there may be an onset of liquid crystalline or crystalline behaviour occurring when octyl chains are present in these systems. This is further discussed in the nanostructure section.

The three samples with low volume after drying all had an octyl chain on either the amine or acid, suggesting a weaker ionisation reaction with increasing alkyl chain length. For the octylamine-nitric

acid combination the decrease in volume was attributed to sample loss during drying in the vacuum oven where the sample appeared to ‘boil’, and in part overflow the vial. Consequently, this acid-base combination cannot be unambiguously determined to have poor proton transfer. However, for the octanoic acid paired with pentylamine or ethanolamine the low volume was most likely due to weak proton transfer. For many PILs, the difference between the aqueous acid and base pK_a values provide a guide to the expected strength of proton transfer.¹¹ For the precursors used in this investigation the pK_a values are approximately 4.8-4.9 for propanoic to octanoic acid, and 10.6 for the alkylamines, 1.3 for nitric acid, and 9.5 for ethanolamine. Based on the aqueous pK_a values it would be forecast that there will be similar proton transfer for all the alkylcarboxylic acid-alkylamine combinations. However, this is not the case for these samples, indicating that the pK_a values in water are not always a sufficient predictor of the prospect of PIL formation. This is consistent with a previous study which showed that amine precursors had different deprotonation abilities towards the dye phenol red, despite similar pK_a values.¹² This is also consistent with precursor acid and bases, and the neat PILs being non-aqueous solvent media where acid-base equilibria will be different to that observed in water.

The water contents of EAF and EAN were measured using Karl Fischer titration after the initial drying in the ISYNTH reactor on the Chemspeed, and found to be 21.5 and 28.7 wt% respectively. Consequently, all 48 acid-base combinations underwent further drying, which was conducted in a vacuum oven at 70-80 °C for approximately 25 hours. The final water contents are provided in Figure 2 in wt%. There was a large variation between 1.02 wt% water for pentylammonium heptanoate and 11.43 wt% water for ethylammonium formate, though most had less than 4 wt% water. The precursors of nitric acid and ethylamine both had 30 wt% water present, however there was no correlation observed for the PILs containing these precursors to have higher water contents.

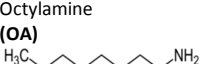
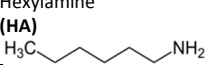
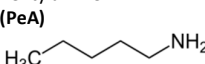
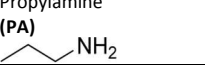
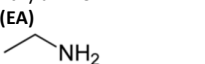
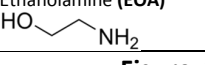
ACIDS \ BASES	Formic (F) 	Acetic (A) 	Propanoic (P) 	Pentanoic (Pe) 	Hexanoic (H) 	Heptanoic (Hep) 	Octanoic (O) 	Nitric (N) 
Octylamine (OA) 	3.20	1.41	H 1.40	H 1.94	H 1.80	1.78 *	1.14	1.52 #
Hexylamine (HA) 	H 1.33	H 1.74	H 1.24	H 1.96	H 2.31	H 1.84	2.30	3.12
Pentylamine (PeA) 	L 1.10	H 1.16	H 1.43	H 1.13	H 1.23	H 1.02	3.65 #	0.97 *
Propylamine (PA) 	L 3.05	M 3.12	M 2.21	M 3.07	H 3.30	H 2.80	H 1.88	L 10.70
Ethylamine (EA) 	L 11.43	7.99 *	M 5.23	H 5.95	M 4.06	M 2.89	M 2.28	L 3.09
Ethanolamine (EOA) 	M 3.18	M 2.13	H 1.82	H 2.54	H 2.34	H 2.07	3.01 #	L 1.55

Figure 2. Summary of the visual state, viscosity and water contents (wt%) of the 48 acid-base combinations. The liquid, gel and solid samples are represented by the heat map with light blue, medium blue and dark blue respectively. The viscosity of the samples was classified as low (L),

medium (M) or high (H) (see text for description of process). The samples which were particularly hygroscopic are denoted with a *, and those where there was a low sample volume by #.

A simple visual screen for the surface tension of the liquid acid-base combinations was developed which consisted of placing a drop onto a microscope glass slide and observing the contact angle. To enable this to be conducted in a HT manner the actual contact angles were not measured, but instead the relative contact angles were compared to the other samples. The drop images for the liquid samples are provided in Figure S2 of the supplementary material. The relative contact angle of the droplets was used to obtain the heat map shown in Figure 3, which classified the acid-base liquids as having a surface tension between very high and very low.

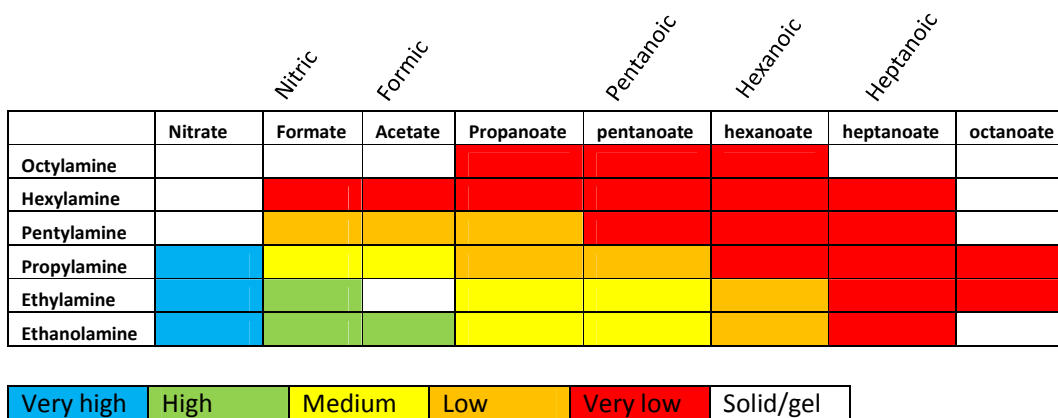


Figure 3. Heat map of the surface tensions for the liquid acid-base combinations.

A bubble tensiometer was used to obtain the surface tension of the liquids to assess the validity of the HT visual screen. The values obtained are provided in Table 1. Due to their high viscosities, higher temperatures were required to enable measurements to be obtained for some samples. Comparison of Figure 3 and Table 1 shows a good correlation, which validates the visual screen conducted for the droplets on a slide. In particular, this screen was successful at identifying the liquids with the highest surface tensions. It is expected that this screen would be valid for the rapid identification of a larger series of ILs, or IL-solvent mixtures with high surface tensions.

Table 1. Surface tension values in mN/m for the liquid acid-base combinations.

	Nitrate	Formate	Acetate	Propanoate	pentanoate	hexanoate	heptanoate	octanoate
Octylamine				30.7 ^b	28.5 ^b	28.7 ^b		
Hexylamine		27.8 ^a		28.9 ^b	32.8 ^b	30.7 ^b	27.9 ^c	
Pentylamine		32.0 ^a	35.1 ^b	27.3 ^c	28.5 ^b	26.2 ^b	28.2 ^b	
Propylamine	39.8 ^a	36.8 ^a	34.5 ^a	32.6 ^a		30.9 ^a	31.4 ^a	40.1 ^a
Ethylamine	47.9 ^a	40.6 ^a		32.7 ^a	31.7 ^a	30.2 ^a	31.6 ^a	29.7 ^a
Ethanolamine	58.4 ^a	53.8 ^a		41.4 ^b	29.4 ^c	29.4 ^c		

^a 22 °C

^b 32 °C

° 37 °C

The surface tensions were observed to roughly decrease with increasing alkyl chain length on either the anion or cation, with ethanalammonium paired with nitrate or formate having significantly higher surface tensions than the other samples. At the air-liquid interface it can be assumed that the ions will orientate such that the charged groups are within the bulk liquid and the alkyl chains are in contact with air. In a previous paper we have reported that increasing the alkyl chain length increases the packing efficiency of the alkyl chains, and hence decreases the surface tension⁹. Based on the symmetry of the heat map in Figure 3, and the values in Table 1, it appears that changing the alkyl chain length on either the cation or the anion generally has a similar effect on the overall surface tension.

Of the 48 acid-base combinations trialled, to the best of our knowledge, only 13 have previously been reported. These were ethylammonium octanoate¹³, ethanalammonium octanoate¹³, ethylammonium nitrate¹⁴, ethylammonium formate⁹, ethylammonium acetate⁹, ethanalammonium nitrate⁹, ethanalammonium formate⁹, ethanalammonium acetate⁹, propylammonium nitrate¹⁵, propylammonium acetate¹⁶, propylammonium formate⁹, pentylammonium formate⁹ and pentylammonium nitrate¹⁷. Direct comparison between the experimental values obtained here and the literature values is difficult due to the higher proportion of water present in these samples. However, the values obtained here were all consistent with the literature, particularly for samples which were solid or liquid, and the expected trends observed for viscosity and surface tension.

Nanostructure

The SAXS/WAXS patterns were acquired for the 45 acid-base combinations which were identified as possible PILs, based on the screen shown in Figure 2. The three that were identified with poor proton transfer were omitted. The use of the Australian Synchrotron SAXS/WAXS beamline enabled the patterns to be acquired rapidly, with an exposure time used of 1 second per sample. With the exception of EOAN and EOAF all the samples contributed a low q peak associated with the presence of polar and non-polar domains, and a second peak at approximately 1.5 \AA^{-1} . Correlation distances, d , were obtained from these peak positions (q) using Bragg's Law, $d=2\pi/q$, in a manner previously described^{17,18}. A summary of the q and d values for the two peaks present for each PIL is provided in Table S3 of the supplementary material. The alkyl chain on the cation and/or anion can segregate to form non-polar domains. The correlation distance, d_1 , can be considered as the distance from the charged headgroup on one ion to the charged headgroup on the second ion which is separated by their alkyl chains, and contributes the low q peak. For most of the ILs which have been investigated in this manner, the alkyl chain is usually located on the cation, and hence the correlation distance, d_1 , is usually across two cations.¹⁹ However, there have been studies where the alkyl chain is on the anion²⁰. The correlation distance, d_2 , is attributed to correlations due to intramolecular interactions and nearest neighbours, and contributes the peak at higher q .

Previously we have reported on the effect of water on the nanostructure of PILs, including some used as part of this investigation, and observed that the addition of significant proportions of water does not affect the peak position of q_1 , though does decrease the peak intensity.²¹ For example, the correlation peaks present in PeAN did not shift for additions of water up to 0.89 molar fraction of

water, and above that the peak could no longer be observed.²¹ The peak position, q_2 , was observed to shift to higher q values with increasing water concentration.²¹

The combined SAXS/WAXS patterns were acquired in a similar manner for a selection of the precursors. Consistent with previous investigations, all of the amines, nitric acid and formic acid had no low q peak present.²¹ In contrast, the selection of acids where the SAXS/WAXS were acquired of acetic, propionic, hexanoic and heptanoic all had a significant low q peak, which is summarised in Table S4 in the supplementary material. The correlation distances, d_1 , present for the neat acids was smaller than that of their counterpart anions when paired with the ethanolammonium cation, which is shown in Figure 4. The ethanolammonium cation was used for the comparison due to it being known that it does not segregate into non-polar domains due to the hydroxyl on the alkyl chain.

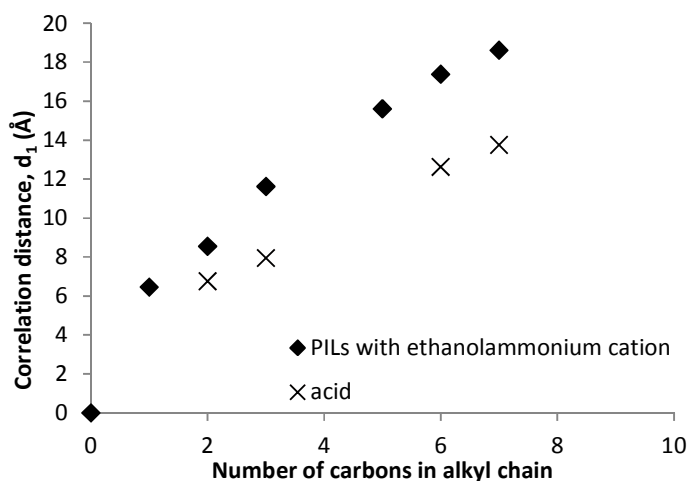


Figure 4. Comparison of the correlation distance, d_1 , present for the neat acids and the PILs containing the ethanolammonium cation paired with the different anions.

The non-polar domain of the nanostructure present for the PILs containing the nitric or formic anion can be considered to be solely due to the alkyl chain on the cation, and conversely for the alkyl chain on the anion when paired with the ethylammonium cation. The SAXS/WAXS patterns for the samples containing the formate anion paired with the ammonium cations are shown in Figure 5a. Similarly the SAXS/WAXS for the series containing the EOA cation paired with the different anions is shown in Figure 5b. The correlation distances, d_1 , corresponding to these two series are provided in Figure 5c. These PILs all show the expected trend of an increasing correlation distance with increasing alkyl chain length^{17,22}. It is apparent from Figure 5c that the contribution of the alkyl chain to the correlation distance is the same regardless of whether it is located on the cation or the anion.

It should be noted that for this comparison we included the carbon of the carboxylate group in the length of the alkyl chain on the anion.

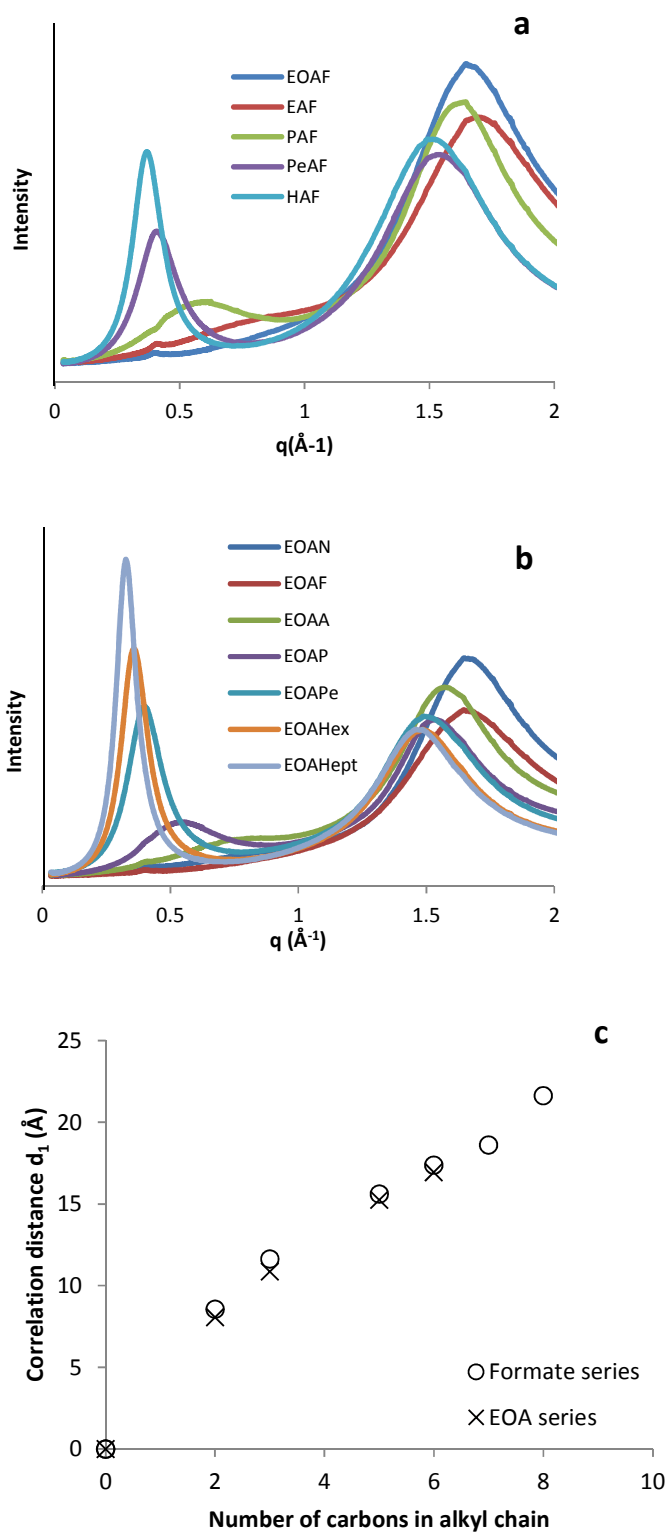


Figure 5. The combined SAXS/WAXS plots for the a) formate anion paired with the different ammonium cations, b) EOA cation paired with the different anions and c) the correlation distances corresponding to the low q peak in (a) and (b) plotted against the number of alkyl chains on either the cation or anion. All data was acquired at 25 °C.

When there is an alkyl chain present on both the cation and the anion then the resulting nanostructure of the PIL depends on both alkyl chain lengths. A representative series of SAXS/WAXS patterns are provided in Figure 6a for the PILs containing the hexylammonium cation paired with the anions used in this investigation. The corresponding correlation distances for the low q peak are provided in Figure 6b. The SAXS/WAXS patterns for the other series of PILs are provided in Figure S3 of the supplementary material, and the correlation distances for all the samples are plotted in Figure 7a against the alkyl chain length on the anion, and similarly in Figure 7b against the alkyl chain length on the cation.

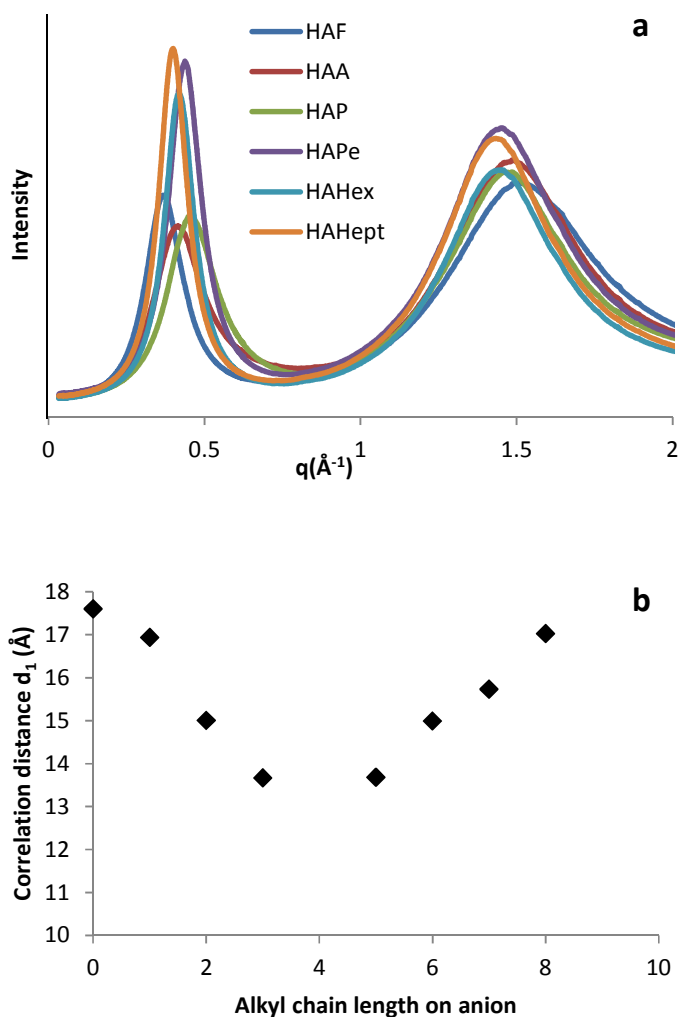


Figure 6. a) SAXS/WAXS patterns for the series of PILs consisting of the hexylammonium cation with the various anions. b) Correlation distances corresponding to the low q peak in (a).

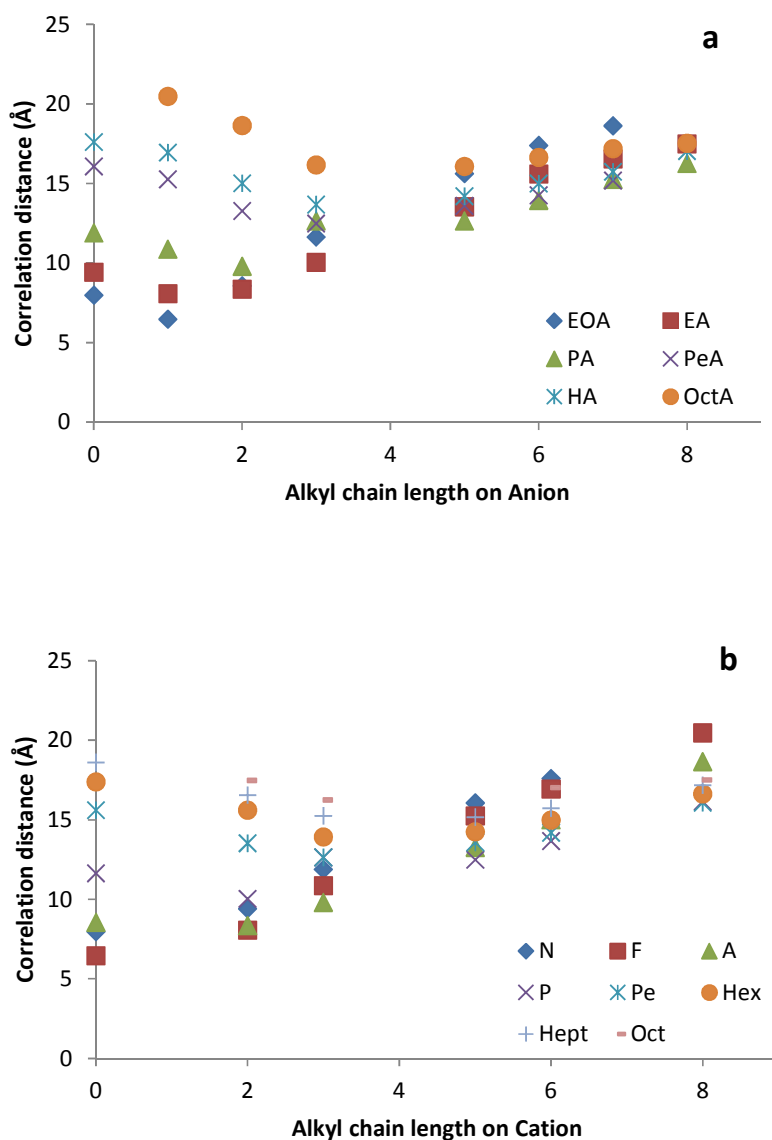


Figure 7. The correlation distances, d_1 , for all the PILs are plotted against the alkyl chain length on a) the anion and b) the cation.

We postulate that there is strong intercalation of the cations and anions, driven by charge alternation of the polar headgroups in the polar region, leading to alternating cations and anions, and alternating alkyl chains in the non-polar region of the respective cations and anions. For aprotic ILs there is typically a peak present around 0.75 \AA^{-1} which is associated with the charge alternation.^{23,24} It is expected that it is not seen in PILs due to the peak and anti-peak contributions cancelling.

A schematic representation for alkyl chain segregation is provided in Figure 8 that is consistent with the changes in the correlation distances based on the alkyl chain lengths present on the cation and anion. The simplest situation is described in Figure 8a where the alkyl chain is only present on one ion, and leads to the largest correlation distances within the samples. The diagram in Figure 8a corresponds to samples HAF or HAN, with the alkyl chain on the cation, or it can correspond to EOA if the charges are reversed, where the alkyl chain is then present on the anion. The schematic shares similarities with cationic or anionic amphiphile liquid crystal structures, with the ion without the alkyl chain behaving as a counterion.

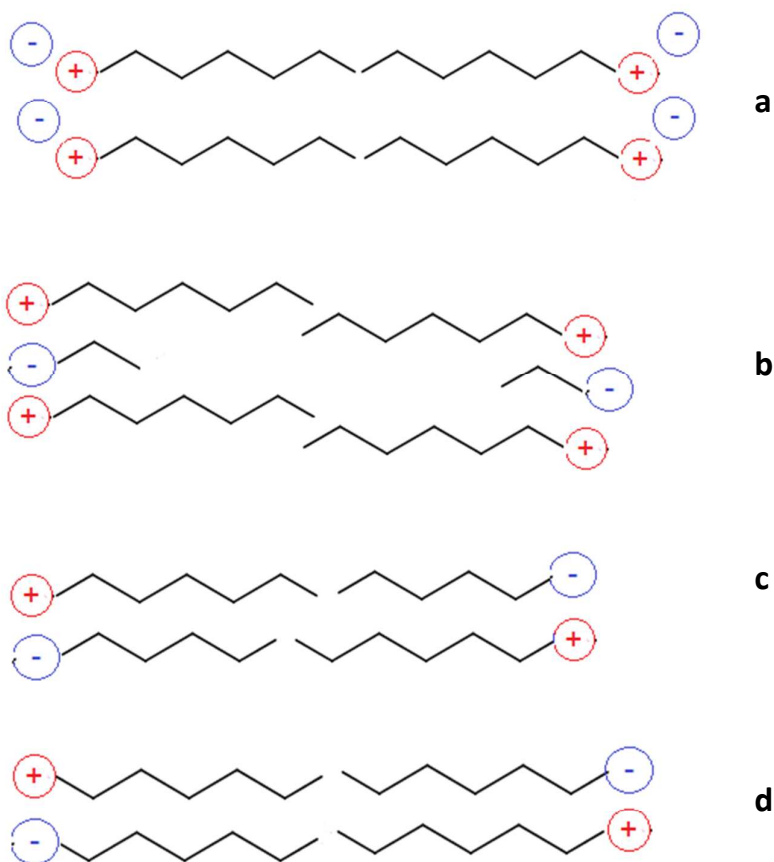


Figure 8. Representation of alkyl chain orientation for a) alkyl chain only present on one ion, b) alkyl chains of significantly different lengths present on cation and anion, c) alkyl chains similar (but

different) on cation and anion in a toe-to-toe orientation, and d) alkyl chain same length for both ions.

We propose that for PILs with different alkyl chain lengths on both ions, the segregation of the alkyl chain is dominated by the longest chain, with the shorter chain adding disorder, and increased interdigitation, illustrated in Figure 8b. Alternatively, if the two chains are similar in length, then both can be expected to contribute more equally to alkyl chain segregation (Figure 8c) leading to smaller correlation distances. It is anticipated that there would also be interdigitation present to some extent for the chains shown in Figure 8c.

Figure 8d contains a schematic for when the alkyl chain is the same on both the cation and the anion, with HAH shown as a representative example. The charge alternation of cations and anions is predicted to lead to an arrangement similar to what is shown. It is evident from Figures 6 and 7 that having the same alkyl chain length on both ions (Figure 8d) leads to a smaller correlation distance than when only one ion contains the alkyl chain (Figure 8a). It was observed that larger correlation distances were obtained when only one ion has the alkyl chain. We suggest that this is in part due to the location of the non-alkyl containing ion, having a greater tendency to locate within the polar region (illustrated in Figure 8a) that a PIL having the same ions but with alkyl chains on both the anion and cation, hence increasing the overall correlation distance.

The schematics shown in Figure 8 represent the proposed ion positions for the series of PILs with a hexylammonium cation, and hence correspond to the correlation distances in Figure 6. We propose that the distinctive minima present in Figure 6, and for many of the series in Figure 7, corresponds to the change in the alkyl chain arrangement between that represented in Figure 8b and 8c, with the specific location of the minima depending on the length of the alkyl chain plotted in the Figure 6.

It was observed using the visual screens that when there was an octyl chain present on either the cation or the anion, that the IL was significantly more likely to be a gel or a solid. We attribute this to an increased van der Waals interaction, and enhanced packing of alkyl chains, enabling crystalline and liquid crystalline phases to form. However, there were some acid-base combinations that formed liquids at room temperature which had an octyl chain on either the anion or cation which includes OAP, OAPe, OAH, PAO and EAO. The listed PILs all are expected to have alkyl chains arranged similar to those represented in Figure 8b or 8c, with significant disorder and intercalation of the alkyl chains. Consequently, the liquid state of these samples is likely a consequence of the alkyl chains being prevented from packing into ordered structured due to this disorder.

Discussion

This investigation resulted in 48 stoichiometric acid-base combinations being reported and dried to a few wt% water content within 96 hours. The samples were prepared in two separate batches of 24, with each having a synthesis time of 7 hours to ensure slow acid addition to the bases, and a drying period of 48+ hours. The characterisation of the PILs in this set of 48 was consistent with the minority group which had previously been reported. Future experiments on similar robotic platforms could be optimised to enable more samples to be prepared within the same time period using

smaller vials, or more heating/cooling modules such as the isynth module used here. Similarly, the experimental conditions could be modified to achieve a lower water content through longer drying times, higher vacuum or higher temperatures during the drying period. We recognise that many of these PILs may be solid at room temperature when rigorously dried. However, their chemical state after the partial drying on the ChemSpeed does provide useful information which is indicative of their future melting point.

For our purposes, these samples were sufficiently dry to enable the identification of the subset of prepared samples which have certain characteristics, such as low melting points, low viscosity and high surface tensions. This smaller subset could then be more rigorously dried and characterised. The nanostructure of PILs such as these has previously been shown to be robust to the addition of water²¹, and hence the SAXS/WAXS patterns could be used to obtain meaningful data on these samples without the need for further drying. The correlation distances, d_1 , associated with the presence of polar and non-polar domains are consistent with the literature for the few PILs which have previously had their nanostructure reported, viz. EOAN, EOAF, EAN, EAF, PAN, PeAN and PeAF (PIL acronyms defined in Figure2).¹⁷

We envisage that future experiments like this would require the development of a range of HT screens to identify solvent characteristics relevant for the desired application. In addition to the melting point, viscosity and surface tension screens included in this investigation, we would expect that HT screens for solvent characteristics such as conductivity, hydrophobicity/hydrophilicity, solvent miscibility and solubility of specific solutes would be relatively simple to develop. We expect that HT screens would be particularly useful for screening ILs consisting of new ions, or ions such as substituted heterocyclic ions where the properties cannot be predicted reliably.

We acknowledge that access to robotic platforms, such as the one used in this experiment is limited. However, many high-throughput techniques are routinely used in biological and materials science fields. We anticipate that some would be adaptable to ILs, and highly suited considering the vast number of cation-anion pairings possible, along with the added dimension of mixing them with one or more solvents or ILs. In particular, we expect that there are many HT methods which could be employed for the preparation of combinatorial arrays of IL-solvent mixtures, and for the screening for specific properties of the resulting solvents.

Of note was the fact that the library of PILs produced had different drying rates depending on their chemical structure. Higher values were expected for PILs containing the ethylammonium cation or nitrate anion as their precursors had 30 wt% water. Although EAN used both of these precursors only 3.09 wt% water was present. The water content of the other precursors was low. We suggest the different drying rates are predominantly due to the hydrophilicity of the PILs and the strength of hydrogen bonding between the PILs and water. This screen for the drying rate of the PILs will enable rapid identification of fast drying ILs with desirable properties.

The field of ILs has been dominated by rigorous investigations into the properties of very small libraries of ILs. We believe that there is a need for an additional process, where a broader range of ILs, or IL-molecular solvents are screened to determine which are likely to have desirable properties. This smaller prospective subset can then be characterised in detail for specific applications. High-

throughput formulation methods should be further considered for preparation IL-molecular solvent mixtures, and where feasible for the preparation of ILs.

Conclusion

A series of 48 stoichiometric combinations of 6 amines and 8 acids was prepared and dried to a few wt% water content by using a robotic platform and a vacuum oven in a fraction of the time of conventional synthesis methods. We report 35 new acid–base combinations in this investigation, and of the initial 48 combinations, 32 can be designated as protic ionic liquids (PILs). This represents a significant increase in the number of known PILs, and highlights the practicality of using high-throughput and combinatorial techniques for the synthesis, formulation and screening of new libraries of PILs, and ionic liquid-solvent mixtures.

The nanostructure of the PILs were characterised using SAXS/WAXS, and to the best of our knowledge this is the first report into the effect of having an alkyl chain present on the cation and the anion. The correlation distance, d_1 , obtained here agreed well with the literature values for the five nanostructured PILs previously reported.

The maximum correlation distance, d_1 , was obtained when there was only an alkyl chain present on either the cation or anion. Increasing the alkyl chain length on the other ion caused d_1 to decrease, which was attributed to disorder in the packing of the alkyl chains, along with increased interdigitation of the longer alkyl chains. As the shorter alkyl chain in the system is increased there is a minimum d_1 present, which has been proposed to occur when there is toe-to-toe alignment of the alkyl chains, such that the non-polar domain contributes the length of the alkyl chain on both the cation and anion.

Visual screens were developed to enable the rapid identification of acid-base combinations that would result in the formation of PILs, and of those which were likely to have low melting points, high surface tensions, low viscosities, and fast drying rates. We would like to emphasise that while the synthesis method required a robotic platform, all of the screens could be simply implemented in any laboratory.

Acknowledgements

Krystal Ha acknowledges CSIRO for the award of a vacation studentship. Some of this research was undertaken on the SAXS/WAXS beamline at the Australian Synchrotron, Victoria, Australia.

Supplementary material is available for the amine-methanol stock solutions, specific volumes dispensed using the Chemspeed robot, the visual appearance of all the samples, the surface tension droplet images, and SAXS/WAXS patterns for all the samples along with the specific correlation peak positions and distances from the SAXS/WAXS patterns.

References

- (1) Aparicio, S.; Atilhan, M.; Karadas, F. *Ind. Eng. Chem. Res.* **2010**, *49*, 9580.
- (2) Feng, R.; Zhao, D.; Guo, Y. *Journal of Environmental Protection* **2010**, *1*, 95.
- (3) Greaves, T. L.; Drummond, C. J. *Chemical Reviews* **2008**, *108*, 206.

- (4) Chatel, G.; Pereira, J. F. B.; Debbeti, V.; Wang, H.; Rogers, R. D. *Green Chem.* **2014**, *16*, 2051.
- (5) Cain, R.; Narramore, S.; McPhillie, M.; Simmons, K.; Fishwick, C. W. G. *Bioorganic Chemistry* **2014**, *55*, 69.
- (6) Nakamoto, H.; Watanabe, M. *Chemical Communications* **2007**, 2539.
- (7) Rebros, M.; Gunaratne, H. Q. N.; Ferguson, J.; Seddon, K. R.; Stephens, G. *Green Chemistry* **2009**, *11*, 402.
- (8) Zavrel, M.; Bross, D.; Funke, M.; Buchs, J.; Spiess, A. C. *Bioresource Technology* **2009**, *100*, 2580.
- (9) Greaves, T. L.; Weerawardena, A.; Fong, C.; Krodkiewska, I.; Drummond, C. J. *Journal of Physical Chemistry B* **2006**, *110*, 22479.
- (10) Zhou, Z. B.; Matsumoto, H.; Tatsumi, K. *Chem. -Eur. J.* **2005**, *11*, 752.
- (11) Yoshizawa, M.; Xu, W.; Angell, C. A. *J. Am. Chem. Soc.* **2003**, *125*, 15411.
- (12) Stoimenovski, J.; Izgorodina, E. I.; MacFarlane, D. R. *Phys. Chem. Chem. Phys.* **2010**, *12*, 10341.
- (13) Shen, Y.; Kennedy, D. F.; Greaves, T. L.; Weerawardena, A.; Mulder, R. J.; Kirby, N.; Song, G.; Drummond, C. J. *Phys. Chem. Chem. Phys.* **2012**, *14*, 7981.
- (14) Walden, P. *Bull. Acad. Imp. Sci.* **1914**, 1800.
- (15) Poole, C. F. *J. Chromatogr.* **2004**, *1037*, 49.
- (16) Hou, M. Y.; Xu, Y. J.; Han, Y. J.; Chen, B.; Zhang, W. X.; Ye, Q. H.; Sun, J. Z. *Journal of Molecular Liquids* **2013**, *178*, 149.
- (17) Greaves, T. L.; Kennedy, D. F.; Mudie, S. T.; Drummond, C. J. *Journal of Physical Chemistry B* **2010**, *114*, 10022.
- (18) Pott, T.; Meleard, P. *Phys. Chem. Chem. Phys.* **2009**, *11*, 5469.
- (19) Greaves, T. L.; Drummond, C. J. *Chem. Soc. Rev.* **2013**, *42*, 1096.
- (20) Russina, O.; Gontrani, L.; Fazio, B.; Lombardo, D.; A., T. *Chemical Physics Letters* **2010**, *493*, 259.
- (21) Greaves, T. L.; Kennedy, D. F.; Weerawardena, A.; Tse, N. M. K.; Kirby, N.; Drummond, C. J. *J. Phys. Chem. B* **2011**, *115*, 2055.
- (22) Triolo, A.; Russina, O.; Bleif, H. J.; Di Cola, E. *Journal of Physical Chemistry B* **2007**, *111*, 4641.
- (23) Kashyap, H. K.; Hettige, J. J.; Annapureddy, H. V. R.; Margulis, C. J. *Chemical Communications* **2012**, *48*, 5103.
- (24) Annapureddy, H. V. R.; Kashyap, H. K.; De Biase, P. M.; Margulis, C. J. *Journal of Physical Chemistry B* **2010**, *114*, 16838.